Online NWP-Model Data as Boundary Conditions for Snow Drift Simulation

Simon Schneiderbauer[1,*] and Stefan Pirker[1]
[1] Institute of Fluid Mechanics and Heat Transfer, Johannes Kepler University, Altenbergerstr. 69, Linz, Austria

ABSTRACT: The open boundary conditions for the computational fluid dynamics simulation of the micro- and meso-scale flow over the Grimming mountain, Austria, are determined by an optimization approach. The Numerical Weather Prediction (NWP) model ALADIN–Austria provides data of wind speed and wind direction at virtual weather balloons within the area of interest. Moreover, the numerical model includes buoyancy, thermal stratification, adiabatic heating and turbulence effects. Furthermore, it is applied to the flow over the Grimming mountain and the results are validated by station data and show suitable correlation with the measurements. In addition, the wavelength of lee gravity waves is in good agreement with analytic approximations and gives an additional validation of the presented model. Finally, the presented model is able to serve as framework for particle transport simulations as snow drift.

KEYWORDS: Open Boundary Conditions, Optimization, Boussinesq approximation, CFD

1 INTRODUCTION

In mountain regions the simulation of micro- and meso-scale wind flows is an important base for particle transport phenomena as snow drift and snow accumulation. The knowledge of the micro-scale wind field and temperature distributions is a key factor for appropriate modeling of snow accumulation, erosion and snow properties, respectively. In Austria two Numerical Weather Prediction (NWP) models are operated by the Central Institute for Meteorology and Geodynamics (ZAMG) that provide a broad range of meteorological data. However, due to the coarse resolution of the NWP models, micro and meso-scale flow features cannot be obtained by these wide range models. Resolving meso-scale wind fields actually requires a three-dimensional Computational Fluid Dynamics (CFD) simulation and cannot be handled by a stratified layer model. Thus, the challenge arises to embed a comprehensive meso-scale CFD simulation into a wide range NWP model.

Thereby, one mayor question is the appropriate definition of time-dependent boundary conditions (BCs) for the meso-scale CFD simulation. Some boundary conditions like the mean flow velocities and the temperature can be extracted from the wide-range NWP model by simple extrapolation. Corresponding extrapolation algorithm should preferably consider reasonable height dependent boundary profiles. Nevertheless, since even the topographies of the ground surface differ between the NWP model and a finely resolved model this one directional interpolation inevitably leads to a significant mass imbalance in the meso-scale model (e.g. Schneiderbauer et al., 2008). Finally, the NWP model data are provided at discrete time-steps in the order of hours. Thus, a time-dependent meso-scale model would also require an interpolation in time.

In this work a mass conserving optimization approach to determine the open boundary conditions is presented. Thereby, the wind speed and direction at virtual stations or “weather balloons” can be deduced from the NWP model by trilinear interpolation (Haiden et al., 2007). While the boundary wind field is defined by this optimization approach the inflow temperature profiles are directly extrapolated from the NWP model.

Moreover, the local wind speeds – especially the shear stresses exerted onto the ground by the flow – and local temperatures are important parameters for an appropriate simulation of snow drift. E.g., the critical shear stress defining the threshold for aerodynamic entrainment strongly depends on the temperature (cf. Schmidt, 1980). In a next step, the resulting wind fields will serve as framework for the snow drift model of Schneiderbauer et al., 2008.

Finally, as an example, the flow over the Grimming mountain is computed by extracting the time dependent open boundary conditions from the NWP model ALADIN (e.g. Wang et al.,

Corresponding author address: Simon Schneiderbauer, Recipient of a DOC-fellowship of the Austrian Academy of Sciences Institute of Fluid Mechanics and Heat Transfer, Johannes Kepler University, Altenbergerstr. 69, Linz, Austria
tel: +43 70 2468 9778
email: simon.schneiderbauer@jku.at

2006). The results are validated by measurement data from a weather station located at a peak (Multereck) of the Grimming massif.

2 MODEL DESCRIPTION

Flow Equations

The commercial CFD solver FLUENT is used to solve the Navier Stokes Equations. In this work constant density is assumed. The turbulent closure is achieved by the RNG k-ε model approach (Choudhury, 1993; Kim and Patel, 2000).

To include buoyancy effects, a transport equation for the temperature T (Energy Equation cf. Fluent 6.2 Manual, chapter 12.2.1) is solved. The closure of the Conservation Equations is done by the continuous Boussinesq approximation

$$\frac{\rho - \rho_0}{\rho_0}\boldsymbol{g} \approx -\beta\big(T - T_0(z)\big)\boldsymbol{g}$$

where ρ_0 is the constant density of the flow, $\boldsymbol{g}$ the standard acceleration of gravity and $T_0(z)$ the operating temperature given from the NWP model. In the presented considerations T_0 is a function of the height z (compare with, e.g., Montavon, 1998) and β denotes the thermal expansion coefficient. The buoyancy term appears as modification of the body forces in the momentum equation.

In addition, in order to take account of adiabatic heating and cooling an energy source E_S is added to the Energy Equation

$$E_S = -c_v \rho \frac{\partial T}{\partial z} w$$

where c_V is the specific heat capacity and w the wind speed in upward direction. Hence, thermal stratification effects like temperature inversions or thermal phenomenons like thermal lifts, thermal air currents (convection), thermal instabilities or gravity winds can be reproduced by the CFD model.

A Mass Conserving Optimization Approach

In this work, we follow the approach for the determination of open boundary conditions proposed by Schneiderbauer and Pirker 2008 or Chu et al. 1997. In first place, the wind speeds $\boldsymbol{\sigma}$ at virtual weather stations are functions of the boundary conditions $\boldsymbol{\varphi}$, which force the system. Since the forward problem of the Navier Stokes equations is given by a non linear operator equation, a solution of

$$\boldsymbol{\sigma}(\boldsymbol{\varphi}, t) = \boldsymbol{\omega}(t) \tag{1}$$

cannot be found explicitly, where $\boldsymbol{\omega}$ are the observed wind speeds at the virtual weather balloons (compare with Figure 2) and t symbolizes the time. An illustration of $\boldsymbol{\varphi}$, $\boldsymbol{\sigma}$ and $\boldsymbol{\omega}$ can be seen in Figure 1. Consequently, Equation (1) is reformulated into an optimization problem. Hence, a cost function is defined by the squared difference of the observations $\boldsymbol{\omega}_i$ and their model analogs $\boldsymbol{\sigma}_i$. In this work, the subscript i indicates the index of the virtual weather balloons and their simulation counterparts. Thus, the cost function reads

$$J(\boldsymbol{\varphi}_1, \boldsymbol{\varphi}_2, \ldots) = \int_{\Delta t} \sum_i \left\| \boldsymbol{\sigma}_i(\boldsymbol{\varphi}_1, \boldsymbol{\varphi}_2, \ldots) - \boldsymbol{\omega}_i \right\|^2 dt \tag{2}$$

where Δt is the time interval of the optimization procedure. Minimizing the cost function respect to $\boldsymbol{\varphi}_j$ leads to a system of equations

$$\sum_i \frac{\partial \boldsymbol{\sigma}_i}{\partial \boldsymbol{\varphi}_j}\big(\boldsymbol{\sigma}_i(\boldsymbol{\varphi}_1, \boldsymbol{\varphi}_2, \ldots) - \boldsymbol{\omega}_i\big) = 0 \tag{3}$$

whereas the gradients can be computed numerically by finite differences (cf. Schneiderbauer and Pirker, 2008). After linearization of Equation (3) the boundary conditions $\boldsymbol{\varphi}_j$, which minimize Equation (2), can be obtained by solving the resulting system of equations.

Furthermore, the vector $\boldsymbol{\omega}_i$ is given by the measurements respectively interpolated ALADIN data of the u and v components of the wind speeds at the balloons. Furthermore, the solutions $\boldsymbol{\sigma}_i$ depend on the parameterization $\boldsymbol{\varphi}_j$ of the inflow and outflow boundary conditions j. For the presented simulations we consider the vectors $\boldsymbol{\varphi}_j$ as horizontal inflow and outflow velocities 10 m above the ground

$$\boldsymbol{\varphi}_j = \begin{pmatrix} u_{10,j} \\ v_{10,j} \end{pmatrix} . \tag{4}$$

Thus, we are led to 8 unknowns taking into account the western (W), northern (N), eastern (E) and southern (S) boundaries (compare with Figure 1). Finally, we assume a logarithmic wind profile for the wind speeds $\boldsymbol{u}_j$ at the boundaries j given by

$$\boldsymbol{u}_j(h) = \boldsymbol{\varphi}_j \frac{\ln h - \ln r}{\ln h_0 - \ln r} \tag{5}$$

where h denotes the height above the ground, $h_0 = 10$ m indicates the reference height, r the surface roughness and $j \in \{\mathrm{W,N,E,S}\}$ (compare with Figure 1).

From Equations (4) and (5) it is clear that the proposed formulation of the inflow and outflow boundary conditions do not preserve mass a priori. Hence, following the continuity equation

$$\nabla \cdot \boldsymbol{u} = 0$$

with $\boldsymbol{u} = (u,v,w)$ a continuity constraint J_C

$$\begin{aligned} J_C &= \int_{\Delta t} \left(\int_V \nabla \cdot \boldsymbol{u}(\varphi_1, \varphi_2, \ldots)\, dV \right)^2 dt = \\ &= \int_{\Delta t} \left(\int_{\partial V} \boldsymbol{u}(\varphi_1, \varphi_2, \ldots) \cdot \boldsymbol{n}\, dS \right)^2 dt \end{aligned}$$

is added to the cost function (2) to fulfill mass conservation. Here $\boldsymbol{n}$ denotes the unit surface normal of the boundary, V the flow volume and ∂V the boundary of V. To sum up, the whole cost function reads

$$\begin{aligned} J &= \int_{\Delta t} \sum_i \| \boldsymbol{\sigma}_i(\varphi_W, \varphi_N, \varphi_E, \varphi_S) - \boldsymbol{\omega}_i \|^2 \\ &\quad + \left(\int_{\partial V} \boldsymbol{u}(\varphi_W, \varphi_N, \varphi_E, \varphi_S) \cdot \boldsymbol{n}\, dV \right)^2 dt \end{aligned}$$

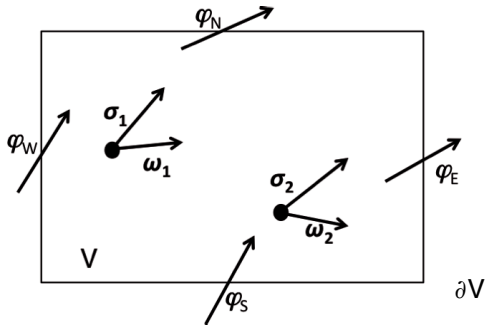

Figure 1. Illustration of the quantities $\boldsymbol{\varphi}_j$, $\boldsymbol{\sigma}_i$ and $\boldsymbol{\omega}_i$; the BCs $\boldsymbol{\varphi}_j$ force the flow (defined on volume V with boundary ∂V) as velocity boundary conditions leading to solutions $\boldsymbol{\sigma}_1$ and $\boldsymbol{\sigma}_2$ at the virtual weather balloons (dots). The quantities $\boldsymbol{\omega}_1$ and $\boldsymbol{\omega}_2$ are the observation counterparts of $\boldsymbol{\sigma}_i$, hence, the interpolated ALADIN velocities at the balloons.

3 UNSTEADY FLOW OVER THE GRIMMING MOUNTAIN

Numerical Grid

For the numerical analysis of the flow over the Grimming mountain a hexahedral finite volume mesh is used. The horizontal extensions of the grid are 10.6 km in west–east direction and 8.8 km in north–south direction. The top boundary is placed 2 km above the crest. The horizontal resolution is 50 m around the crest, which is linearly expanded by 12% towards the boundaries. In Figure 2 the horizontal stretching of the grid is shown. The first cell layer above the surface level is of constant thickness of about 1 m, which is sufficient to obtain acceptable results for the flow quantities near the surface (cf. Undheim et al., 2006; Castro et al., 2003). The vertical stretching from the surface to the top of the grid is set to 12%. The total number of grid cells is 53×46×50.

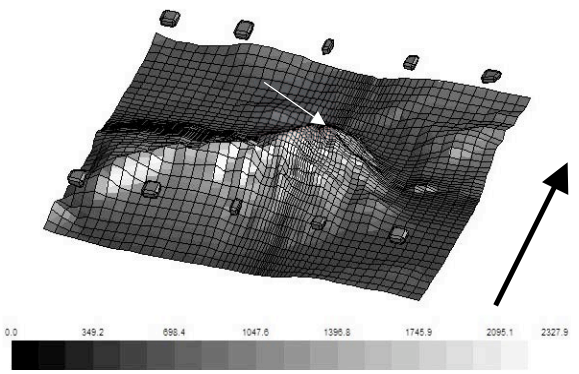

Figure 2. Horizontal distribution of the grid cells around the Grimming mountain used in the simulations. The colorbar indicate the elevation in m and the arrow points northwards. The gray ashlars correspond to the virtual weather balloons and the white arrow to the reference station at 2170 m a.s.l.

Boundary Conditions

At the top boundary the flux and the gradients of all flow variables are set to zero. At the bottom boundary a no slip boundary condition is applied. The temperature at the bottom boundary is given by the interpolated and extrapolated ALADIN–Austria fields, respectively. At the western, northern, eastern and southern boundaries the wind speed and direction is given by Equations (4) and (5). The pressure gradient at these boundaries is set to zero. At the inflow boundaries, which are identified by the optimization algorithm, the temperature is determined similarly to the bottom boundary. The turbulence quantities are provided from a two dimensional simulation.

Results

The unsteady wind field around the Grimming mountain is computed based on an hourly ALADIN–Austria forecast, which starts at Monday, the 18th of August 2008, at midnight.

In Figure 3 the time series of the wind speeds at the reference station are shown. One

can see clearly from the Figure, that the optimization algorithm updates the boundary conditions hourly. To validate the results, the wind speed, wind direction and temperature are compared with measured data at a reference station, which is not incorporated into the optimization procedure. The location of the reference station is shown in Figure 2. Up to $t = 3$ h the simulated wind speed is in satisfactory agreement with the station measurements, which is displayed in Figure 3. The computed wind speed (solid line) is mostly between or hardly below the measured 30 min average and the measured wind peaks in the corresponding 30 min intervals. From $t = 3$ h to $t = 4$ h the ALADIN forecast does not predict the decrease in wind speed. Thus, the simulated wind speed differs significantly from the measured data within this period. In Figure 4 the computed wind direction at the reference station is shown. Over the whole period the simulation results fit the measured data in an acceptable way.

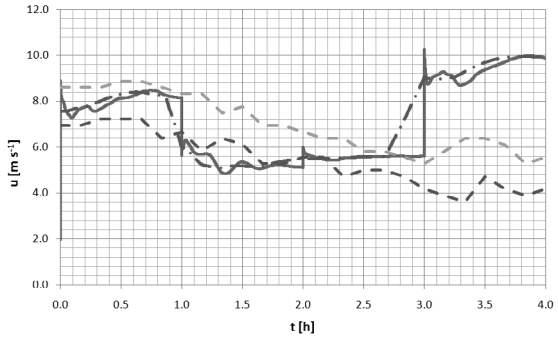

Figure 3. Wind speed at the reference station (solid line: computed wind speed; dashed dotted line: 30 min floating average of the computed wind speed; lower dashed line: 30 min floating average of the measured wind speed; upper dashed line: wind peaks within 30 min intervals)

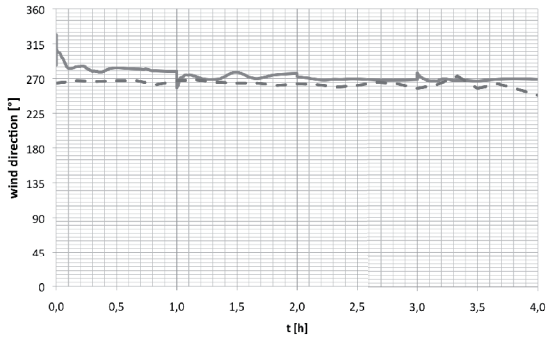

Figure 4. Wind direction at the reference station (solid line: computed wind direction; dashed line: measured wind direction; N ≡ 0°, E ≡ 90°, S ≡ 180°, W ≡ 270°)

In Figure 5 the time series of the temperature at the reference station is shown. As before, the simulation results are quite good connected to the measured data. The discontinuities at $t = 1$ h and $t = 3$ h correlate with the unsteadiness of the wind speed (Figure 3). Nevertheless, the presented results give a quantitative measure of the temperature distribution around the crest defining an important parameter for snow erosion and sedimentation processes (e.g. Gauer, 1999). Moreover, in Figure 6 the temperature distribution at 10 m height from west to east crossing the reference station is shown. It can be clearly seen, that the temperature correlates with the height above the sea level by adiabatic heating and cooling, respectively.

Finally, in the atmospheric flow internal gravity waves can be induced by surface features. Consequently, the characteristics of gravity waves are a measure of the quality of the model. A common approximation of the wavelength of gravity lee waves (mountain waves) in the atmosphere is given by (cf. Eliassen and Kleinschmidt, [1957])

$$\lambda = 2\pi \|\boldsymbol{u}\| \sqrt{\frac{T}{g(\vartheta_d - \vartheta)}}$$

$\vartheta_d = [illegible]$ and $\vartheta = [illegible]$ denote the dry adiabatic and the environmental lapse rates derived from the ALADIN temperature profile, respectively. For $u = 4$ m s^{-1} and $T = 273$ K, obtained from the simulation, the wavelength of the lee gravity wave is about $\lambda \approx 2.3$ km. From Figure 7 we get a wavelength of about 2.5 km.

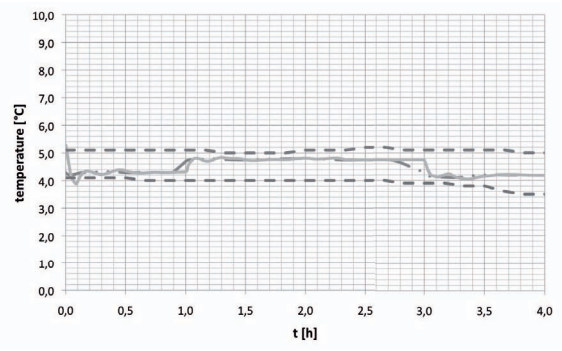

Figure 5. Temperature in °C at the reference station (solid line: computed air temperature; dashed dotted line: 30 min floating average of the computed air temperature; lower dashed line: measured air temperature; upper dashed line: measured air temperature at a snow gauge 50 m below the crest)

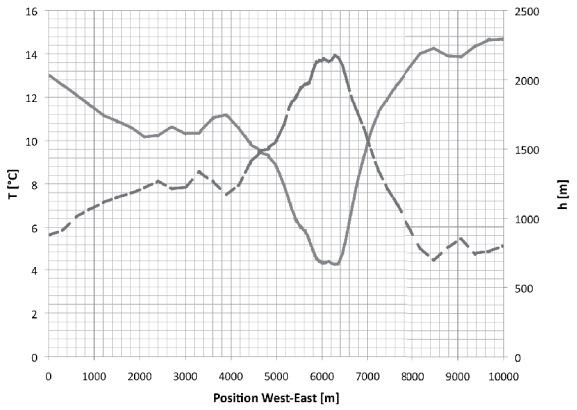

Figure 6. Temperature in °C (solid line) at h = 10 m above the ground from west to east crossing the reference station at t = 1 h. The dashed line corresponds to the elevation of the mountain.

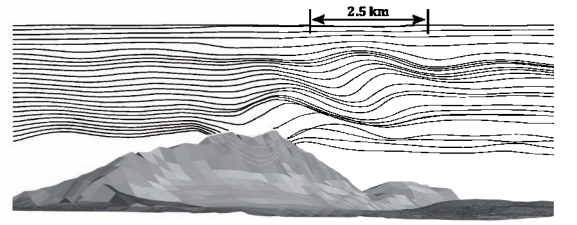

Figure 7. Pathlines of massless particles released from the west.

4 CONCLUSIONS AND OUTLOOK

In this paper it has been shown, that the determination of open boundary conditions from macro- and meso-scale NWP models by optimization techniques for micro-scale alpine wind field computations seems to be a good tool to detect local wind and temperature conditions. Additional physical models that take account of buoyancy, turbulence, adiabatic heating and thermal stratification effects are included. By using a mass preserving optimization approach to determine the boundary conditions, the local conditions are reproduced by the model, which is validated by station measurements. Nevertheless, additional work has to be done on the discontinuities induced by the huge difference in the time scales of the ALADIN output (hourly) and the simulation (seconds). Here, an interpolation in time of the ALADIN fields may lead to smoother time series of the micro-scale wind fields. Finally, the presented model provides a quantitative measure of the flow over the Grimming mountain. Hence, this model is a base for e.g. snow drift simulations, reproducing micro-scale wind patterns or computing wind loads on alpine buildings.

5 REFERENCES

Castro, F. A., Palma, J. M. L. M. and Silva Lopes, A., 2003. Simulation of the Askervein Flow. Part 1: Reynolds averaged Navier-Stokes Equations (k-ϵ Turbulence Model). Boundary-Layer Meteorology, 107:501-530.

Choudhury, D., 1993. Introduction to the Renormalization Group Method and Turbulence Modeling. Fluent Inc. Technical Memorandum TM-107.

Chu, P. C., Fan, C., and Ehret, L. L., 1997. Determination of Open Boundary Conditions with an Optimization Method. Journal of Athmospheric and Oceanic Technology, 14:723-734.

Eliassen, A. and Kleinschmidt, E., 1957. Handbuch der Geophysik, Band XLVIII, chapter Dynamic Meteorology, pages 1–154. Springer Verlag.

Fluent 6.2 Manual, 2005. Fluent 6.2 User's Guide.

Gauer, P., 1999. Blowing and Drifting Snow in Alpine Terrain: A Physically-Based Numerical Model and Related Field Measurements. PhD thesis, SLF Davos.

Haiden, T., Kann, A., Pistotnik, G., Stadlbacher, K., Steinheimer M., Wimmer, F. and Wittmann, C., 2007. Integrated Nowcasting through Comprehensive Analysis (INCA) — System Overview. Zentralanstalt für Meteorologie und Geodynamik, Wien.

Kim, H. G., Patel, V. C., and Lee, C.M., 2000. Numerical simulation of wind flow over hilly terrain. Journal of Wind Engineering and Industrial Aerodynamics, 87:45-60.

Montavon, C.,1998. Validation of a non-hydrostatic numerical model to simulate stratified wind fields over complex topography. Journal of Wind Engineering and Industrial Aerodynamics, 74–76:273-282.

Schmidt, R.A., 1980. Threshold wind-speeds and elastic impact in snow transport. Journal of Glaciology, 26(94):453–467.

Schneiderbauer, S. and Pirker, S., 2008. Determination of Open Boundary Conditions for Computational Fluid Dynamics (CFD) from a Numerical Weather Prediction (NWP) model. submitted to Applied Mathematical Modelling.

Schneiderbauer, S., Tschachler, T., Fischbacher, J., Hinterberger, W. and Fischer, P., 2008. CFD Simulation of Snow Drift in Alpine Environments for Operational Avalanche Warning Including a Local Weather Model. Annals of Glaciology, 48:150-158.

Undheim, O., Andersson, H. I. and Berge, E., 2006. Non-Linear, microscale modelling of the flow over Askervein hill. Boundary-Layer Meteorology, 120:477-495.

Wang, Y., Haiden, T. and Kann, A., 2006. The Operational Limited Area Modelling System at ZAMG:ALADIN-AUSTRIA. Österreichische Beiträge zu Meterologie und Geophysik, 37:4.